submitted to ACS Nano, Dec. 2017

Vibrational Changes Induced by Electron Transfer in Surface Bound Azurin Metalloprotein Studied by Tip-Enhanced Raman Spectroscopy and Scanning Tunneling Microscopy

Stefan Kradolfer[1#], Ewelina Lipiec[1, 2#], Chiara Baldacchini[3, 4#], Anna Rita Bizzarri[3], Salvatore Cannistraro[3], Renato Zenobi[1*]

[1]Laboratory of Organic Chemistry, Department of Chemistry and Applied Biosciences, ETH Zurich, 8093 Zurich, Switzerland

[2] The Henryk Niewodniczanski Institute of Nuclear Physics, Polish Academy of Sciences 31-342 Krakow, Poland

[3] Biophysics and Nanoscience Centre, DEB, Università della Tuscia, I-01100 Viterbo, Italy

[4] Institute of Agro-Environmental and Forest Biology, CNR, I-05010 Porano, Italy

[#] these authors contributed equally to this work

*correspondence to: zenobi@org.chem.ethz.ch

Abstract: The copper protein azurin, due to the peculiar coupling of its optical and vibronic properties with electron transfer (ET) and its biorecognition capabilities, is a very promising candidate for bioelectronic, bio-optoelectronic and biosensor applications. However, a complete understanding of the fundamental processes relating azurin ET, and its optical and vibronic characteristics with the charge transport mechanisms occurring in proteins bound to a conductive surface, the typical scenario for a biosensor or bioelectronic component, is still lacking. We studied azurin proteins bound to a gold electrode surface by scanning tunneling microscopy combined with tip-enhanced Raman spectroscopy (STM-TERS). Robust TER spectra were obtained, and the protein's vibronic response under optical excitation in resonance with its ligand-to-metal charge transfer band was found to be affected by the tunneling parameters, indicating a direct involvement of the active site vibrations in the electron transport process.

Keywords: STM-TERS, azurin, metallo-proteins, charge transfer, electron-phonon interaction.

Redox metalloproteins are biocompatible nanoscale objects endowed with electron transfer (ET) capabilities[1] and have attracted attention for a long time, in view of possible applications in

bioelectronic devices.[2] In particular, the blue copper protein azurin has generated significant interest[3-6] due to its peculiar redox, optical and vibrational properties,[7] its significant robustness, and its biorecognition capabilities towards several biomolecules, including the oncosuppressor p53.[8,9]

Azurin is a 14.6 kDa monomeric type I copper (Cu) protein (Figure 1a) involved in the shuttling of electrons within the respiratory transport chain of *Pseudomonas Aeruginosa* bacteria.[10-12] During ET under physiological conditions, the Cu ion in the active site switches between two oxidation states (Cu^{2+}/Cu^{1+}), and the electron is transferred across the protein along a well defined pathway, encompassing the polypeptide chain, some of the hydrogen bonds, and the tryptophan residue at position 48 (Trp48).[13-15] The Cu ion is five-fold coordinated with three strong equatorial ligands (N^{δ} of His46 and His117 and S^{γ} of Cys112) and two more weakly bonded axial ligands (S^{δ} of Met121 and the backbone oxygen of Gly45), resulting in a distorted trigonal bipyramidal geometry (Figure 1b).[7] This peculiar symmetry is finely tuned by the vibrational "quake" induced by the docking of the partner, which facilitates the occurrence of physiological ET.[16] The peculiar Cu ion-ligand symmetry in the active site is responsible for both the high azurin redox potential, and the ligand field energy levels that give rise to the typical d-d optical transitions of the protein.[7] These transitions coalesce into an intense ligand-to-metal charge transfer (LMCT) absorption band peaking at about 620 nm.[7] Optical excitation in resonance with this band activates the azurin active site vibrations,[17, 18] as witnessed by the peculiar resonance Raman spectrum,[19] characteristic of the oxidized (Cu^{2+}) state of the protein.[20]

** Fig. 1 here **

A very interesting, and somewhat intriguing interplay exists among azurin's ET mechanism, its optical absorption transitions, and the active site vibronic properties. Furthermore, azurin's remarkable robustness ensures that both its ET and its biorecognition capabilities are maintained upon adsorption on surfaces.[6] This renders this protein a biocompatible nano object that is highly suitable for applications in bioelectronics, bio-optoelectronics and biosensors. To fully control and

efficiently tailor azurin's conduction characteristics within hybrid nannostructures, the fundamental processes connecting azurin's electronic, optical, and vibrational characteristics with the charge transport mechanisms upon conjugation with conductive electrodes, should be better understood.[21,22] It has already been shown that charge transport across single azurin molecules bound to conductive electrodes can be controlled by tuning the protein's electrochemical potential[23-28] and the local charging,[6, 29] or by optically exciting the protein in resonance with its LMCT band.[30] However, the role played by the protein's phonons, and in particular by the active site vibrations, in sustaining charge transport across the nanostructure is still unclear. Indeed, it has been reported that stress-induced structural modification may affect the azurin's conductivity,[31-35] but a direct involvement of active site's vibrations in charge transport across solid state azurin has been excluded.[36]

We have investigated the interdependence between protein phonons and charge transport in azurin molecules bound to a gold electrode, by performing a combined scanning tunneling microscopy/tip-enhanced Raman spectroscopy (STM-TERS) investigation.[37] In particular, we have focused on the copper-containing active site's vibronic response upon charge transfer, by optically exciting the protein in resonance with its LMCT absorption band. The resonant STM-TERS spectra of chemisorbed azurin are presented here, and were found to replicate the typical resonance Raman spectrum of bulk azurin in solution, confirming that the entangled geometry of the Cu ion within the active site and, thus, the electronic, optical and vibrational properties of azurin, are preserved upon conjugation with a gold electrode. Nonetheless, changes in the active site vibrational modes occur at specific tunneling conditions, suggesting a direct involvement of the Cu ion energy levels in the charge transport across the hybrid nanostructure.

Results and Discussion

Figure 2 shows STM images of single azurin molecules deposited on a gold surface upon continuous scanning, at an applied voltage of -0.5 V. On the time scale of few tens on minutes,

upon continuous scanning at fixed applied voltage, azurin proteins progressively disappear from the STM images (Figure 2a-2c).

** Fig. 2 here **

Figure 2d shows an AFM image of a ≤ 1 monolayer coverage or azurin that was used for recording the TERS data. It is fairly unstructured, suggesting that a compact monolayer of azurin was present.

** Fig. 3 here **

The typical resonance Raman (RR) spectrum of azurin in solution is shown in Figure 3a. It is characterized by three main features (~369 cm^{-1}, ~408 cm^{-1}, ~424 cm^{-1}) that correspond to the well-known resonant vibrational modes of the oxidized (Cu^{2+}) azurin active site. They are coupled to a single electron transition, namely, the $S_{Cys}\,\sigma\rightarrow$Cu charge-transfer transition, and originate from the kinetic coupling of the (Cu-S_{Cys}) stretching mode, with internal vibrations of the cysteine ligand side chain.[7,17,18,38] Two minor active site related structures are also visible at ~260 cm^{-1} (Cu-N_{His} vibrations) and ~750 cm^{-1} (C-S_{Cys} stretching vibration).[17,38] Interestingly, the same features characterize the RR spectrum of a dried drop of azurin deposited on a gold surface (Figure 3a). This suggests that the structure of the protein active site, which is responsible for its peculiar optical properties, is preserved upon drying and deposition. Moreover, since the Cu ion coordination is an entatic state resulting from a delicate balance involving the folding of the whole protein, [39, 40] its preservation further suggests that the entire protein structure is close to that in physiological conditions. The preservation of the protein conformation upon deposition on the gold surface is further verified by comparing the RR spectrum of dried azurin with the confocal Raman spectrum acquired from the same sample at a different wavelength (532 nm) (Figure 3b**)**. While the RR signal from the Cu-center is much stronger than any other protein-related vibrational mode, the typical protein vibrational features such as the amide bands (at about 1250-1270 cm^{-1} and 1660 cm^{-1}) and the phenylalanine band (at about 1004 cm^{-1}) are clearly visible off-resonance, being even more intense than the Cu-S related stretching modes.

The investigation of the Cu center vibrations upon single-molecule mediated charge transfer requires submonolayer coverages, which does not allow the collection of confocal Raman spectra. TERS permits the Cu-S and Cu-N vibrational modes to be detected with the required sensitivity, although only excitation in resonance with the azurin LMCT band allowed us to obtain strong STM-TER spectra (V_{bias} = 0.2 V, $I_{setpoint}$ = 0.1 nA) from azurin monolayers on a gold surface (Figure 3a). STM-TERS spectra obtained from different samples and using different tips show the same vibrational features in the 350-450 cm^{-1} range, which closely resemble those characterizing the RR spectra of azurin in solution, with a high reproducibility in the peak positions. The observation of such bands suggests that the structure of the azurin active site, and of the whole protein, together with its vibrational properties, are still preserved when azurin chemisorbs to the gold surface, as recently suggested by theoretical investigations. [41]

** Fig. 4 here **

To check the stability of the signal intensity upon irradiation, STM-TER spectra (V_{bias}= 0.2 V, $I_{setpoint}$ = 0.1 nA) were continuously recorded on the same sample spot. Averaged STM-TER spectra, acquired just after approaching the surface (black line) and after 30' (red line), are compared in Figure 4a. These spectra were collected with one and the same tip, and therefore they were not normalized before averaging. The TER signal intensity of the three main RR features significantly decreases with time (left inset in Figure 4a), while no changes are observed in the signal-to-noise ratio (right inset in Figure 4a). By integrating the TER signal intensity in the spectral range from 350 cm^{-1} to 450 cm^{-1}, a net loss of about the 50% of the total intensity is obtained, between the two averaged spectra. Single TER spectra collected one after another over ~ 7 minutes (Figure 4b), and the corresponding TER signal intensity values (integrated over the 350-450 cm^{-1} spectral range; Figure 4c), demonstrate that the TER signal intensity loss is continuous, and that it levels out at ≈50% of the initial value after about 4 minutes.

Factors related with tip or sample degradation, such as changes in tip activity, fluorescence bleaching, or protein degradation, could be responsible of the intensity loss. However, tip degradation could be ruled out, since the tips were observed to remain active after measuring STM-TER spectra from different sample spots, over comparable times. Also fluorescence bleaching can be excluded, since it would have been observed in the whole spectral range,[42] and also because the noise level of the spectra remains constant over time (inset in Figure 4a). Protein decomposition would lead to both a continuous decrease of the TERS signal and to the appearance of amorphous carbon related bands at about 1350 cm^{-1} - 1600 cm^{-1},[43] which are absent (inset in Figure 4a); this confirms the protein's stability against irradiation. The Raman scattering cross-section of carbonaceous contamination is exceptionally high and even slight traces of carbon products of thermal decomposition of the sample would be easily detectable by TERS or/and SERS.[43]

We therefore suggest the long-term intensity loss to be due to a reduction of the (Cu^{2+}) ion in the active site, due to the charges flowing through the molecules under the application of an external bias. Indeed, it is known that only azurin in its oxidized (Cu^{2+}) state exhibits a resonance Raman spectrum, which disappears when reduction to the (Cu^{1+}) state occurs.[20] Interestingly, the time scale of the TER signal intensity loss is reminiscent of that characterizing the fading of the STM images of single azurin proteins on gold surfaces upon continuous scanning, at applied voltage lower than 1.0 V, which was attributed to the progressive charging of the protein milieu.[6] This is consistent with the data reported in Figure 2: on the time scale of few tens on minutes, upon continuous scanning at fixed applied voltage, azurin proteins marked by the white arrows progressively disappear from the STM image. Moreover, the application of very high voltages to the protein (higher than 3.0 V) has been reported to rapidly and reversibly block the charge transport through azurin molecules on gold surfaces.[29] Thus, the timescale of protein charging seems to depend on the ratio between the net electron flux induced through the protein and its electron transfer capability, also considering the high capacitance displayed by the protein when embedded in nanostructures.[29,44] This aspect would deserve further investigations, but it is worth noting that these

experimental evidences further suggest the existence of an interplay between the active site vibrational properties (and related ET capability) and charge transport efficiency across azurin assembled on a gold surface.

STM-TER spectra of azurin monolayers on gold obtained under various tunneling currents and at two different applied voltages are shown in Figure 5, compared with the RR spectrum of a dried drop of azurin. In the STM-TER spectra collected at V_{bias} = 0.2 V, the positions of the resonance vibrations are significantly ($p<0.05$) shifted, by about 4 cm^{-1}, towards higher energies with respect to the dried drop RR spectrum, to ~372 cm^{-1}, ~409 cm^{-1} and ~429 cm^{-1} (Figure 5a). These shifts, which are independent of the setpoint current, could either be due to a Stark effect induced by the applied electric field, which has already been observed in STM-TERS measurements,[45-48] or to charging within the protein,[48] or both. We could rule out that the shift is due to a modification of the active site structure due to the tip intrusion since it is similarly observed at any setpoint current, *i.e.*, at different tip-to-surface distances. When the applied bias voltage is raised to 0.4 V, the spectral shape drastically changes compared to both the RR spectrum and the STM-TER spectra at V_{bias} = 0.2 V (Figure 5). Interestingly, the spectral intensity decreases, new spectral features appear, and the position of the peaks changes with the setpoint current. In addition to the above mentioned Stark and charging effects the appearance of new spectral features, together with the current dependence of the peak positions, would suggest the occurrence of conformational changes in the area including the azurin active site.[7] We can again rule out that these modifications are due to tip intrusion, since we already excluded it at V_{bias} = 0.2 V and, at a comparable setpoint current, the higher the applied voltage, the larger the tip-to-sample distance (and, thus, the lower the tip intrusion) is expected to be.

** Fig. 5 here **

TER spectra from azurin monolayers on gold acquired under the same current ($I_{setpoint}$ = 0.1 nA), at various values of the bias voltage (in the 0.2 – 2.0 V range) were further compared (Figure 6). The spectra collected at applied voltages of 1.0 V and 2.0 V are very similar to those collected at V_{bias} =

0.2 V, well reproducing the vibrational structure of the protein in a dried droplet, without applied voltages and current flow, apart from the already mentioned shift that is likely due to local charging. Among the large data set we collected with several tips on different samples, and exploring many tunneling conditions, the protein vibrational response observed at V_{bias} = 0.4 V appears to be rather special. Moreover, it depends on the tunneling current (Figure 5), which affects the tip-to-sample distance and, hence, the applied electric field. The overall experimental evidence suggests that the differences in protein's vibrational response are connected with the charge transfer occurring across the protein.

** Fig. 6 here **

In STM, when no bias voltage would be applied, the Fermi energy levels (E_F) of the metallic tip and substrate are aligned (Figure 7a).[46] The azurin electronic molecular levels are assumed to be pinned at the substrate E_F, due to the azurin-gold coupling,[27] and the gold E_F is aligned at half energy between the closest occupied and unoccupied molecular energy levels (HOMO and LUMO, respectively), which are mainly related to the active site. According to Marcus' theory, the molecular electronic levels can be assumed to have a broadening of 0.3 eV,[24] and an energy gap between HOMO and LUMO that is twice the activation energy for charge exchange, also called reorganization energy λ.[27] By assuming that λ is similar in STM and in electrochemical ET,[25] its value can be estimated to be about 0.5 eV,[27] with a resulting HOMO-LUMO gap of about 1.0 eV (Figure 7a), which reduces to 0.7 eV taking into account the molecular electronic level broadening. At V_{bias} = 0.2 V, the substrate's E_F is shifted with respect to the tip's E_F, but the latter is still aligned with the HOMO-LUMO gap, allowing only non-resonant tunneling processes between tip and substrate (Figure 7b). In this picture, electrons flow through the protein like across a continuum dielectric medium, possibly inducing molecular charging effects, consistent with the peak intensity loss and the position shifts previously discussed.

** Fig. 7 here **

On the contrary, when V_{bias} = 0.4 V, the tip's E_F is aligned with the azurin LUMO and a two-step resonant tunneling can occur (Figure 7c), with a direct involvement of the protein active site electronic levels in the charge transport.[23-25,27,29] In this case, charge transport is expected to be coupled with the ET capabilities of the protein and charges injected into the Cu ion may flow across the protein following specific ET pathways, which could exit from the Cu ion either through the Cu-S_{Cys112} or through the Cu-N_{His46} bonds.[14] In this context, the differences observed in the resonance vibrational patterns by changing the setpoint current could be interpreted in terms of the activation of different ET pathways across the protein, which differently affect the vibrational richness of azurin's active site, as a function of the tunneling parameters. Finally, when V_{bias} exceeds the energy difference between the protein LUMO and the substrate E_F (Figure 7d), a switch towards non-resonant tunneling is expected.

Thus, under specific energy level alignment conditions, charge transport through an azurin monolayer adsorbed on gold appears to be strongly coupled with the protein active site vibrations, somewhat in disagreement with what has been claimed for a solid state azurin nanodevice.[36]

Conclusions

The high sensitivity of STM-TERS allowed us to investigate the vibronic response of azurin, a blue copper protein, on a gold surface, upon optical excitation in resonance with the protein LMCT absorption band and under controlled charge transport conditions. The vibrational profiles obtained confirm that azurin's active site preserves its conformation upon adsorption. Different vibrational responses to the tunneling current are observed by properly tuning the applied bias voltage, likely due to the switching of the tunneling mechanism in and out from the resonance condition. In non-resonant tunneling, the STM-TERS spectra reproduce the vibrational characteristics of the azurin active site well, and a long-time standing loss of signal intensity, coupled with a small, but reproducible shift of the peak positions towards higher energies, suggest that charging and electrostatic field related effects occur within the protein milieu. A drastic change of the active site vibronic response is indeed associated with resonant tunneling, likely due to the direct involvement

of the active site in the charge transport and to the activation of different ET pathways as a function of the tunneling parameters. Theoretical investigations are in progress, in order to describe the interplay between specific pathways and ET efficiency, also in connection with the resulting vibrational features of the active site.

Methods

Sample preparation. Wild type azurin was prepared and purified as described in Ref.[49] Azurin solutions in MilliQ water at different concentrations were used. The resonance Raman spectrum of azurin in solution was obtained by a 50 mM solution. Bulk samples for confocal resonance Raman spectroscopy were prepared by depositing 40 µl of a 85 mM azurin solution on a gold substrate (Arrandee™, 11x11mm), which were subsequently dried in a constant flow of nitrogen. Protein monolayers suitable for STM-TERS measurements were obtained by depositing 10 µl of a 4 mM azurin solution on a gold substrate, and then storing it for 5 min under vacuum (< 50 mbar) for a fast and homogeneous drying process.[50] Samples were measured immediately after the deposition.

Etching of STM tips. Silver tips were prepared by electrochemical etching from silver wires (diam. 250 µm; ≥99.998%, Alfa Aesar Premion).[51] The etching solution was a 4:1 (v/v) mixture of ethanol (≥99.8 %, Fluka) and perchloric acid (70%, Sigma Aldrich). The tip was immersed approx. 1 mm into the solution in the middle of a platinum ring (diam. approx. 1 cm) as counter electrode, which was held at a potential of 10 V and a current of 10 mA. An electronic control circuit (built in house; ETHZ) cut the applied voltage when the tip lost contact with the solution. Etched tips were rinsed first with milliQ water (NANOpure DiamondTM, Barnsted) and then with ethanol.

STM of individual azurin molecules. Some STM data were recorded on very sparsely covered gold surfaces, which allowed individual azurin molecules to be observed. The sample was prepared by depositing an azurin solution (100 µM in ammonium acetate buffer solution, pH 4.6) on an annealed Au surface (Arrandee) overnight at 4 °C. It was then gently washed with milliQ water and dried in a pure nitrogen flux. The STM data were obtained using a PicoLE 5100 STM (Agilent

Technologies), using $I_{setpoint}$ = 0.06 nA and V_{bias} = -0.5 V.

Raman and STM-TER spectroscopy. Raman spectra of azurin in solution were recorded by a confocal Raman spectrometer (Labram, Jobin-Yvon/Horiba, Villeneuve d'Ascq, France) equipped with a Peltier-cooled charge coupled device (CCD) detector, and a single-grating spectrograph with an 1800 g/mm grating. The microscope objective had a 100× magnification and a numerical aperture of 0.9, producing a laser spot size of about 1μm in diameter. The excitation light source was a HeNe ion laser providing a 633 nm radiation, with a power that was kept below 5mW.

Confocal Raman and STM-TER spectra of dry azurin on gold were obtained by an integrated scanning tunneling microscope and Raman spectrometer (NTEGRA, NTMDT, Zelenograd, Russia) system, in an up-right configuration. For the Raman excitation, either a focused HeNe laser (633 nm, red) or a solid state laser (532 nm, green) was used. All spectra were collected using an acquisition time between 0.5 and 50 s per spectrum, with a laser power of 0.025-1.2 mW (633 nm) or 0.3–1.6 mW (532 nm) on the sample stage. The spectral resolution was approximately 1 cm^{-1}. STM-TERS measurements were done in a constant current mode, with a setpoint current ($I_{setpoint}$) in the range from 0.04 to 5 nA, and a bias voltage applied to the gold surface (V_{bias}) in the range from 0.01 to 3.0 V. The tip enhancement (for every single tip) was determined by scanning the laser beam over the tip with a resolution of approx. 250 x 250 nm per pixels. On the spot with the highest enhancement, the laser was fixed, and this arrangement was used for further measurements. The values of measurement parameters were determined by the spectral quality related to the enhancement of the electromagnetic field for a particular tip.

Data treatment. For data treatment and representation of the spectra, the open source software R (version: 3.1.3 – ©2015 R Foundation for Statistical Computation) implemented in RStudio (Version 0.98.1103 – ©2009-2014 RStudio), OPUS (6.5 Build: 6, 5 (20070524); Bruker Optik GmbH) and OriginPro (2016G (64-bit) Sr1 b9.3.1.273 ©1991-2015 OriginLab Corporation) were used.

TERS signal intensities strongly depend on the shape of the probe apex. Therefore, the spectral intensity as well as the signal-to-noise ratio can be different in sets of spectra measured with different tips. Therefore, smoothing and normalization of the acquired data were done. Spectra were smoothed (Savitzky-Golay algorithm, number of smoothing points: 9-21 depends on the quality), and then baseline corrected (concave rubberband correction, sec. order polynomial, 1-12 iterations). Finally, before averaging of spectra acquired with various tips, a vector normalization was applied within the spectral range from 310 cm^{-1} to 506 cm^{-1}.

Acknowledgments

This work has been partially financed by the PRIN 2012NRRP5J project of the Italian Ministry for University and Research and by the AIRC project n°IG15866. The authors are grateful to C. W. Beattie from the University of Illinois, College of Medicine, Chicago (IL, USA) for kindly providing highly purified azurin protein.

References

(1) Winkler, J. R.; Gray, H. B. Electron Flow through Metalloproteins. *Chem. Rev.* **2013**, *114*, 3369–3380.

(2) Willner, I.; Willner, B. Biomaterials Integrated with Electronic Elements: en Route to Bioelectronics. *Trends Biotechnol.* **2001**, *19*, 222–230.

(3) Davis, J. J.; Morgan, D. A.; Wrathmell , C. L.; Axford , D. N.; Zhao J. Molecular Bioelectronics. *J. Mat. Chem.* **2005**, *22,* 2160–2174.

(4) Artés, J. M.; López-Martínez, M.; Díez-Pérez, I.; Sanz, F.; Gorostiza P. Nanoscale Charge Transfer in Redox Proteins and DNA: Towards Biomolecular Electronics. *Electrochim. Acta* **2014**, *140,* 83–95.

(5) Amdursky, N.; Sepunaru, L.; Raichlin, S.; Pecht, I.; Sheves, M.; Cahen, D. Electron Transfer Proteins as Electronic Conductors: Significance of the Metal and Its Binding Site in the Blue Cu Protein Azurin. *Adv. Sci.* **2015**, *2*, 1400026.

(6) Baldacchini, C.; Bizzarri, A. R.; Cannistraro, S. Electron Transfer, Conduction and Biorecognition Properties of the Redox Metalloprotein Azurin Assembled onto Inorganic Substrates. *Eur. Polymer J.* **2016**, *83*, 407–427.

(7) Solomon, E. I.; Hadt, R. G. Recent Advances in Understanding Blue Copper Proteins. *Coord. Chem. Rev.* **2011,** *255,* 774–789.

(8) Bonanni, B.; Bizzarri, A. R.; Cannistraro, S. Optimized Biorecognition of Cytochrome c 551 and Azurin Immobilized on Thiol-Terminated Monolayers Assembled on Au(111) Substrates. *J. Phys. Chem. B* **2006,** *110,* 14574–14580.

(9) Domenici, F.; Bizzarri, A. R.; Cannistraro, S. Surface-Enhanced Raman Scattering Detection of Wild-Type and Mutant p53 Proteins at Very Low Concentration in Human Serum. *Anal. Biochem*. **2012,** *421*, 9–15.

(10) Nar, H.; Messerschmidt, A.; Huber, R.; van de Kamp, M.; Canters, G. W. Crystal Structure Analysis of Oxidized *Pseudomonas Aeruginosa* Azurin at pH 5.5 and pH 9.0. A pH-Induced Conformational Transition Involves a Peptide Bond Flip. *J. Mol. Biol.* **1991**, *221*, 765–772.

(11) Vijgenboom, E.; Busch J. E.; Canters, G. W. *In Vivo* Studies Disprove an Obligatory Role of Azurin in Denitrification in *Pseudomonas Aeruginosa* and Show that Azu Expression is Under Control of RpoS and ANR. *Microbiol.* **1997**, *143*, 2853–2863.

(12) Vargo, M. L.; Gulka, C. P.; Gerig, J. K.; Manieri, C. M.; Dattelbaum, J. D.; Marks, C. B; Lawrence, N. T.; Trawick, M. L.; Leopold, M. C. Distance Dependence of Electron Transfer Kinetics for Azurin Protein Adsorbed to Monolayer Protected Nanoparticle Film Assemblies. *Langmuir* **2009**, *26*, 560–569.

(13) Farver, O.; Pecht, I. Long Range Intramolecular Electron Transfer in Azurins. *J. Am. Chem. Soc.* **1992**, *114*, 5764–5767.

(14) Farver, O.; Jeuken, L. J. C.; Canters, G. W.; Pecht, I. Role of Ligand Substitution on Long-Range Electron Transfer in Azurins. *Eur. J. Biochem.* **2000**, *267*, 3123–3129.

(15) Shih, C.; Museth, A. K.; Abrahamsson, M.; Blanco-Rodriguez, A. M.; Di Bilio, A. J.; Sudhamsu, J.; Crane, B. R.; Ronayne, K. L.; Towrie, M.; Vlcek Jr., A. *et al.* Tryptophan-Accelerated Electron Flow through Proteins. *Science* **2008**, *320*, 1760–1762.

(16) Bizzarri, A. R.; Cannistraro, S. Electron Transfer in Metalloproteins. In *Encyclopedia of Condensed Matter Physics;* Bassani, G., Liedl, G., Wyder, P., Eds.; Elsevier, 2005**;** pp 361-369.

(17) Webb, M. A.; Kwong, C. M.; Loppnow G. R. Excited-State Charge-Transfer Dynamics of Azurin, a Blue Copper Protein, from Resonance Raman Intensities. *J. Phys. Chem. B* **1997**, *101*, 5062–5069.

(18) Cimei, T.; Bizzarri, A. R.; Cannistraro, S.; Cerullo, G.; De Silvestri, S. Vibrational Coherence in Azurin with Impulsive Excitation of the LMCT Absorption Band. *Chem. Phys. Lett.* **2002**, *362*, 497–503.

(19) Bizzarri, A. R.; Andolfi, L.; Taranta, M.; Cannistraro, S. Optical and Electronic Coupling of the Redox Copper Azurin on ITO-Coated Quartz Substrate. *Biosens. Bioelectron.* **2008**, *24,* 204–209.

(20) Gaigalas, A. K.; Niaura, G. J. Measurement of Electron Transfer Rates between Adsorbed Azurin and a Gold Electrode Modified with a Hexanethiol Layer. *J. Coll. Interf. Sci.* **1997**, *193*, 60–70.

(21) Amdursky, N.; Marchak, D.; Sepunaru, L.; Pecht, I.; Sheves, M.; Cahen, D. Electronic Transport via Proteins. *Adv. Mat.* **2014**, *26,* 7142–7161.

(22) Bostick, C. D.; Mukhopadhyay, S.; Pecht, I.; Sheves, M.; Cahen, D.; Lederman, D. Protein Bioelectronics: a Review of What We Do and Do Not Know. *arXiv* **2017** 1702.05028.

(23) Friis, E.P.; Andersen, J.E.T.; Kharkats, Y. I.; Kuznetsov, A.M.; Nichols, R.J.; Zhang J.-D.; Ulstrup, J. An Approach to Long-Range Electron Transfer Mechanisms in Metalloproteins: *In situ* Scanning Tunneling Microscopy with Submolecular Resolution. *Proc. Nat. Acad. Sci. USA* **1999**, *96*, 1379–1384.

(24) Facci, P.; Alliata, D.; Cannistraro, S. Potential-Induced Resonant Tunneling through a Redox Metalloprotein Investigated by Electrochemical Scanning Probe Microscopy. *Ultramicrosc.* **2001**, *89*, 291-298.

(25) Chi, Q.; Farver, O.; Ulstrup, J. Long-range Protein Electron Transfer Observed at the Single-Molecule Level: *In Situ* Mapping of Redox-Gated Tunneling Resonance. *Proc. Nat. Acad. Sci. USA* **2005**, *102*, 16203–16208.

(26) Choi, J.-W.; Oh, B.-K.; Kim, Y. J. Protein-Based Biomemory Device Consisting of the Cysteine-Modified Azurin. *Appl. Phys. Lett.* **2007**, *91*, 263902.

(27) Artés, J. M.; Dìez-Pérez, I; Gorostiza, P. Transistor-Like Behavior of Single Metalloprotein Junctions. *Nano Lett.* **2012**, *12*, 2679–2684.

(28) Wu, H.; Feng, X.; Kieviet, B. D.; Zhang, K.; Zandvliet, H. J. W.; Canters, G. W.; Schön, P. M.; Vancso, G. J. Electrochemical Atomic Force Microscopy Reveals Potential Stimulated Height Changes of Redox Responsive Cu-Azurin on Gold. *Eur. Polymer J.* **2016**, *83,* 529 – 537.

(29) Baldacchini, C.; Kumar, V.; Bizzarri, A. R.; Cannistraro, S. Electron Tunnelling through Single Azurin Molecules Can Be On/Off Switched by Voltage Pulses. *Appl. Phys. Lett.* **2015,** *106,* 183701.

(30) Baldacchini, C.; Bizzarri, A. R.; Cannistraro, S. Excitation of the Ligand-to-Metal Charge Transfer Band Induces Electron Tunnelling in Azurin. *Appl. Phys. Lett.* **2014**, *104*, 09370.

(31) Davis, J. J.; Wang, N.; Morgan, A.; Zhang, T.; Zhao, J. Metalloprotein Tunnel Junctions: Compressional Modulation of Barrier Height and Transport Mechanism. *Faraday Disc.* **2006**, *131*, 167-179.

(32) Bonanni, B.; Andolfi, L.; Bizzarri, A. R.; Cannistraro, S. Functional Metalloproteins Integrated with Conductive Substrates: Detecting Single Molecules and Sensing Individual Recognition Events. *J. Phys. Chem. B* **2007**, *111*, 5062–5075.

(33) Li, W.; Sepunaru, L.; Amdursky, N.; Cohen, S. R.; Pecht, I.; Sheves, M.; Cahen, D. Temperature and Force Dependence of Nanoscale Electron Transport via the Cu Protein Azurin. *ACS Nano* **2012**, *6*, 10816-10824.

(34) Raccosta, S.; Baldacchini, C.; Bizzarri, A. R.; Cannistraro, S. Conductive Atomic Force Microscopy Study of Single Molecule Electron Transport through the Azurin-Gold Nanoparticle System. *Appl. Phys. Lett.* **2013**, *102*, 203704.

(35) Zhang, X. Y.; Shao, J.; Chen, Y.; Chen, W.; Yu, J.; Wang, B.; Zheng, Y. The Dynamic Conductance Response and Mechanics-Modulated Memristive Behavior of the Azurin Monolayer under Cyclic Loads. *Phys. Chem. Chem. Phys.* **2017**, *19*, 6757-6767.

(36) Yu, X.; Lovrincic, R.; Sepunaru, L.; Li, W.; Vilan, A.; Pecht, I. ; Sheves, M.; Cahen, D. Insights into Solid-State Electron Transport through Proteins from Inelastic Tunneling Spectroscopy: The Case of Azurin. *ACS Nano* **2015**, *9*, 9955-9963.

(37) Sonntag, M. D.; Klingsporn, J. M.; Garibay, L. K.; Roberts, J. M.; Dieringer, J. A.; Seideman, T.; Scheidt, K. A.; Jensen, L.; Schatz, G. C.; Van Duyne, R. P. Single-Molecule Tip-Enhanced Raman Spectroscopy. *J. Phys. Chem. C* **2012**, *116*, 478–483.

(38) Czernuszewicz, R.S.; Fraczkiewicz, G.; Zareba, A. A. A Detailed Resonance Raman Spectrum of Nickel(II)-Substituted *Pseudomonas Aeruginosa* Azurin. *Inorg. Chem.* **2005**, *44*, 5745-5752.

(39) Zong, C.; Wilson, C. J.; Shen, T.; Wittung-Stafshede, P.; Mayo, S. L.; Wolynes, P. G. Establishing the Entatic State in Folding Metallated *Pseudomonas Aeruginosa* Azurin. *PNAS* **2007**, *104,* 3159 –3164.

(40) Fowler, N. J.; Blanford, C. F.; Warwicker, J.; de Visser, S. P. Prediction of Reduction Potentials of Copper Proteins with Continuum Electrostatics and Density Functional Theory. *Chem. Eur. J.* **2017**, *23*, 15436–15445.

(41) Bizzarri, A. R.; Baldacchini, C.; Cannistraro, S. Structure, Dynamics, and Electron Transfer of Azurin Bound to a Gold Electrode. *Langmuir*, **2017**, *33*, 9190–9200.

(42) Laucks, M. L.; Roll, G.; Schweiger, G.; Davis, E. J. Physical and Chemical (RAMAN) Characterization of Bioaerosols-Pollen. *J. Aerosol. Sci.* **2000**, *31*, 307–319.

(43) Domke, K. F.; Zhang, D.; Pettinger, B. Enhanced Raman Spectroscopy: Single Molecules or Carbon? *J. Phys. Chem. C* **2007**, *111*, 8611–8616.

(44) Bueno, P. R.; Fabregat-Santiago, F.; Davis, J. J. Elucidating Capacitance and Resistance Terms in Confined Electroactive Molecular Layers. *Anal. Chem.* **2013**, 85, 411−417.

(45) Suydam, I. T.; Snow, C. D.; Pande, V. S.; Boxer, S. G. Electric Fields at the Active Site of an Enzyme: Direct Comparison of Experiment with Theory. *Science* **2006**, *313*, 200-204.

(46) Hipps, K. W. *Handbook Appl. Solid State Spectrosc*; Vij D. R., Eds.; Springer Science + Business Media, LLC: New York, 2006; pp 305-350.

(47) Marr, J. M.; Schultz, Z. D. Imaging Electric Fields in SERS and TERS Using the Vibrational Stark Effect. *J. Phys. Chem. Lett.* **2013**, *4*, 3268−3272.

(48) Li, Y.; Zolotavin, P.; Doak, P.; Kronik, L.; Neaton, J. B.; Natelson, D. Interplay of Bias-Driven Charging and the Vibrational Stark Effect in Molecular Junctions. *Nano Lett.* **2016**, *161*, 104−1109.

(49) Yamada, T.; Goto, M.; Punj, V.; Zaborina, O.; Chen, M. L.; Kimbara, K.; Majumdar, D.; Cunningham, E.; Das Gupta, T. K.; Chakrabarty, A. M. Bacterial Redox Protein Azurin, Tumor Suppressor Protein p53, and Regression of Cancer. *Proc. Nat. Acad. Sci. USA* **2002**, *99*, 14098–14103.

(50) Blum, C.; Schmid, T.; Opilik, L.; Weidmann, S.; Fagerer, S. R.; Zenobi, R. Understanding Tip-Enhanced Raman Spectra of Biological Molecules: a Combined Raman, SERS and TERS Study. *J. Raman Spectrosc.* **2012**, *43*, 1895–1904.

(51) J. Stadler, J.; Schmid, T.; Zenobi, R. Nanoscale Chemical Imaging Using Top-Illumination Tip-Enhanced Raman Spectroscopy. *Nano Lett.* **2010**, *10*, 4514–4520.

Figure Captions

Figure 1. Chemical structure of azurin: a) crystal structure taken from the X-ray structure at 1.93Å resolution (chain B of PDB entry 4AZU).[10] b) Cu center and neighboring ligands.

Figure 2. (a-c) STM images (60 x 60 nm) of the same region of a gold surface with single

chemisorbed azurin proteins. With respect to the image in panel (a), images in panel (b) and (c) were acquired after 5 and 10 minutes, respectively, of continuous scanning, at the same tunneling conditions ($I_{setpoint}$ = 0.06 nA, V_{bias} = -0.5 V). More details on similar experiments have been reported elsewere.[6] (d) A representative image of an azurin monolayer on a gold surface, obtained by tapping-mode atomic force microscopy (Nanoscope IIIa/Multimode SPM, Digital Instruments). Vertical scale: 5.0 nm; lateral image size: 500 nm.

Figure 3. (a) Comparison of confocal resonance Raman (RR, 633 nm) spectrum of dry bulk azurin on a gold surface with the RR spectrum of an azurin solution (50mM in MilliQ water, 633 nm) and STM-TER spectra of azurin monolayers on gold surfaces as obtained by exciting the proteins in resonance with their LMCT band (633 nm), at the same tunneling conditions (V_{bias}= 0.2 V, $I_{setpoint}$ = 0.1 nA), on different samples and by using different TERS active tips. (b) Comparison of confocal resonance Raman (633 nm, red) spectrum of dry bulk azurin on a gold surface with the confocal Raman spectrum acquired from the same sample at a different wavelength (532 nm, green).

Figure 4. (a) Averaged STM-TER spectra with standard deviation of azurin monolayers on gold surfaces as obtained by exciting the proteins in resonance with their LMCT band (633 nm), at the same tunneling conditions (V_{bias}= 0.2 V, $I_{setpoint}$ = 0.1 nA). Spectra were collected at the beginning (black) and at the end (red) of a 30-mins continuous exposure to the 633 nm laser. (b) STM-TERS spectra acquired on the same sample spot as (V_{bias}= 0.2 V, $I_{setpoint}$ = 0.1 nA) in the 320-480 cm^{-1} spectral range over 7 mins. (c) Total intensity of TER signal from spectra in panel (b), in the spectral range 350-450 cm^{-1}, as a function of a time.

Figure 5. Resonance Raman spectrum or azurin prepared as a dried droplet (633 nm, black trace) and averaged and normalized TER spectra from an azurin monolayer on a gold surface, collected under various values of current at 0.2 V (blue) and 0.4 V (red). Averaged peak positions are shown with their standard deviation. Averaged spectra were obtained from a total number of 73 spectra, collected with 7 different tips.

Figure 6. Averaged and normalized TER spectra from an azurin monolayer on a gold surface collected under a tunneling current $I_{setpoint}$ = 0.1 nA, at various values of the bias voltage: 0.2 V (blue), 0.4 V (red), 1.0 V (green) and 2.0 V (purple).

Figure 7. Schematic energy level diagrams of the tip-azurin-substrate system without applied bias (V_{bias} = 0.0 V) (a), at V_{bias} = 0.2 V (b), at V_{bias} = 0.4 V (d), at V_{bias} = 1.0 V (b). Tip and substrate Fermi energy levels (E_F) are indicated. Unoccupied and occupied electronic molecular levels (MLs, LUMO and HOMO) are symbolized by empty and full rectangles, respectively. The arrows indicate non-resonant (b, d) and resonant (c) electron tunneling.

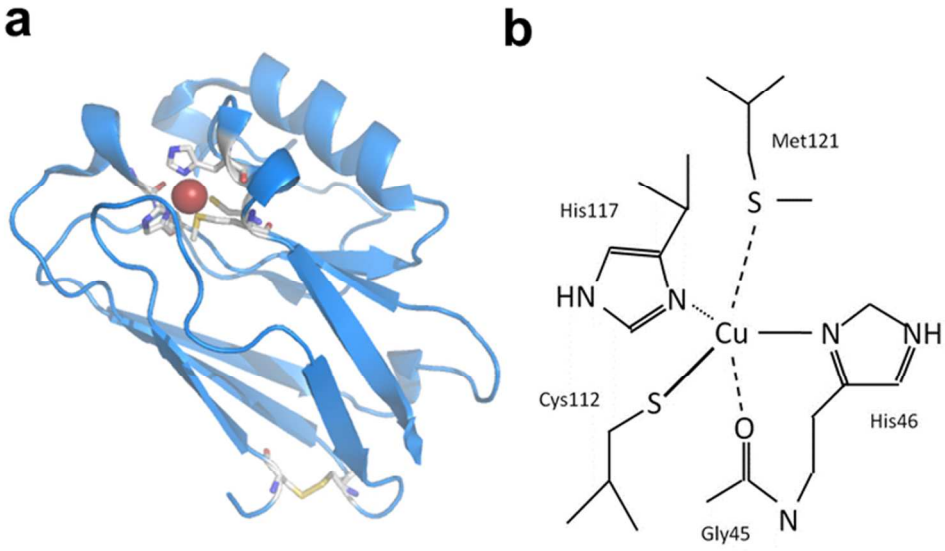

Fig. 1

80x45mm (300 x 300 DPI)

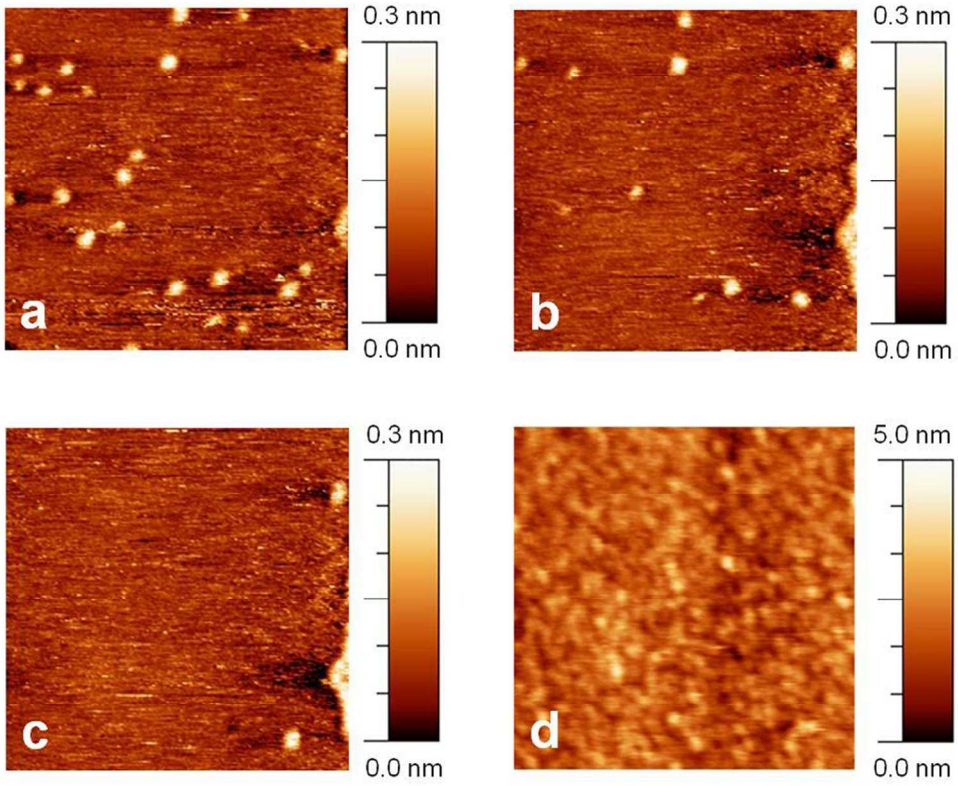

Fig. 2

85x71mm (300 x 300 DPI)

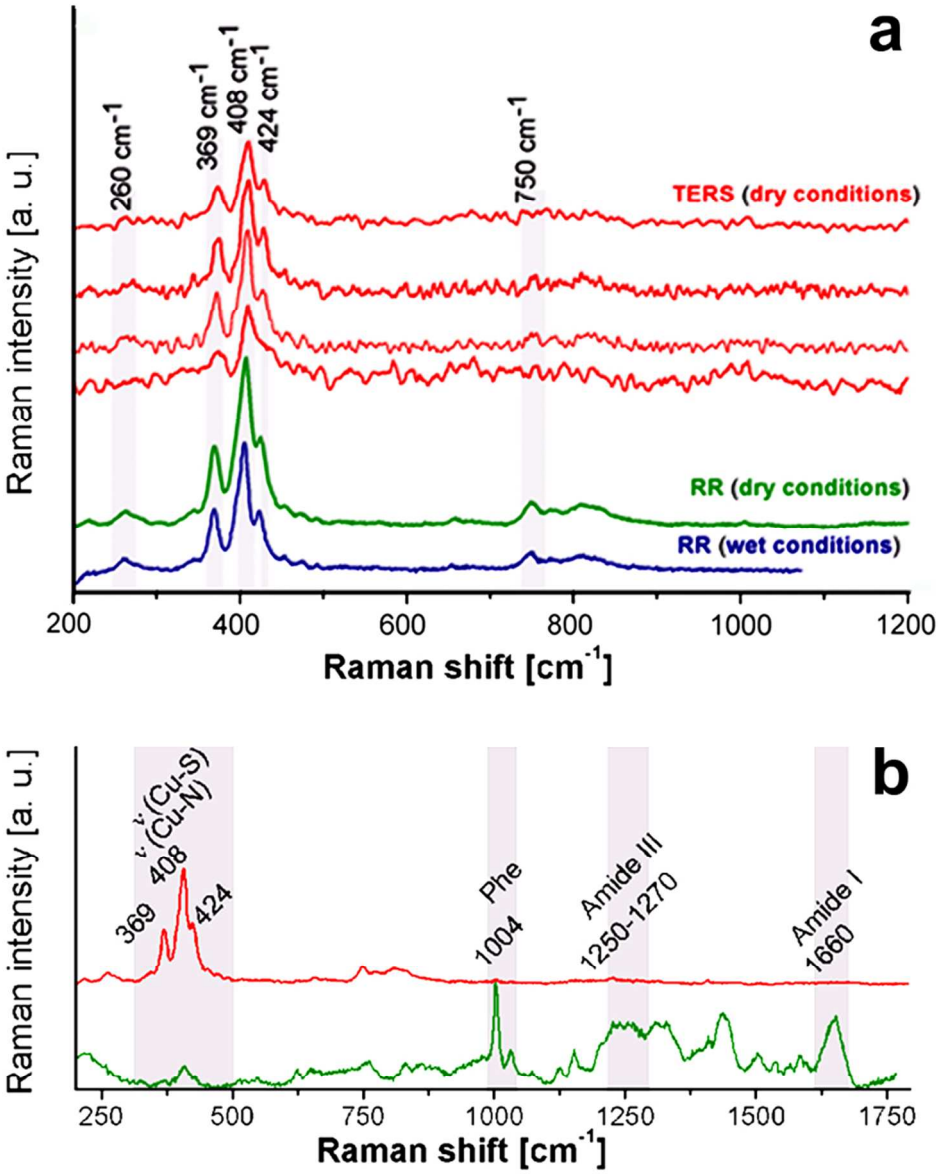

Fig. 3

80x99mm (300 x 300 DPI)

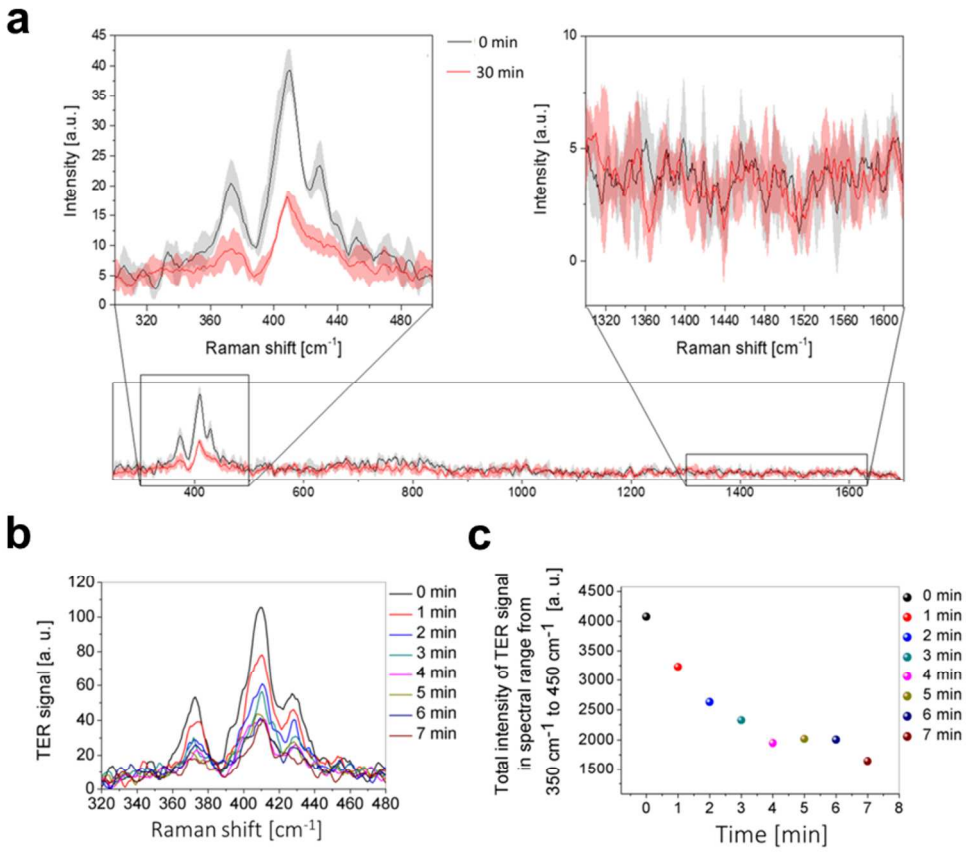

Fig. 4

170x146mm (300 x 300 DPI)

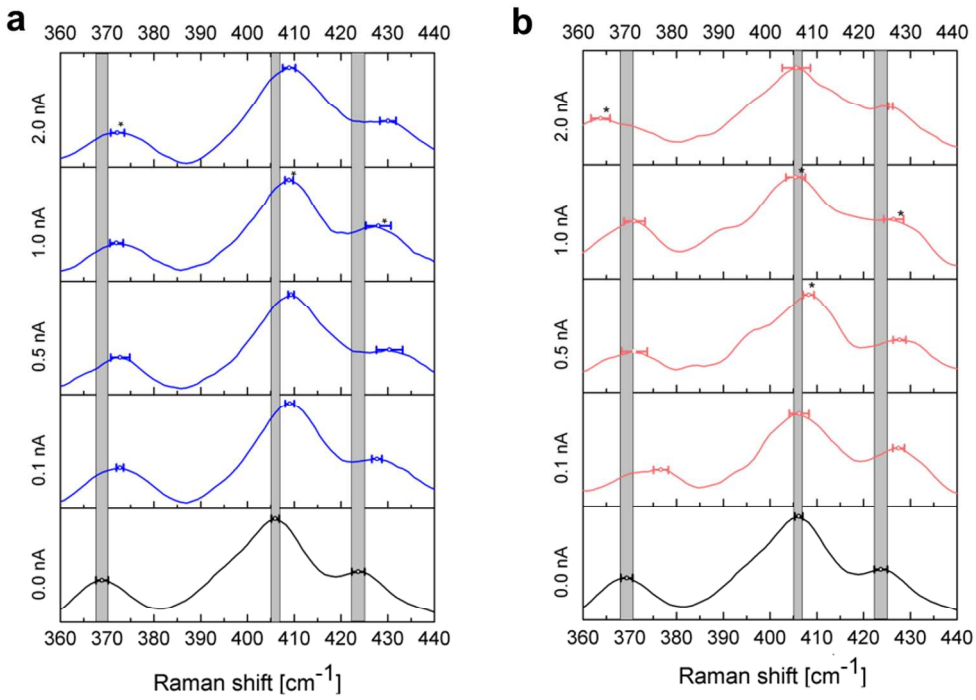

Fig. 5

170x119mm (300 x 300 DPI)

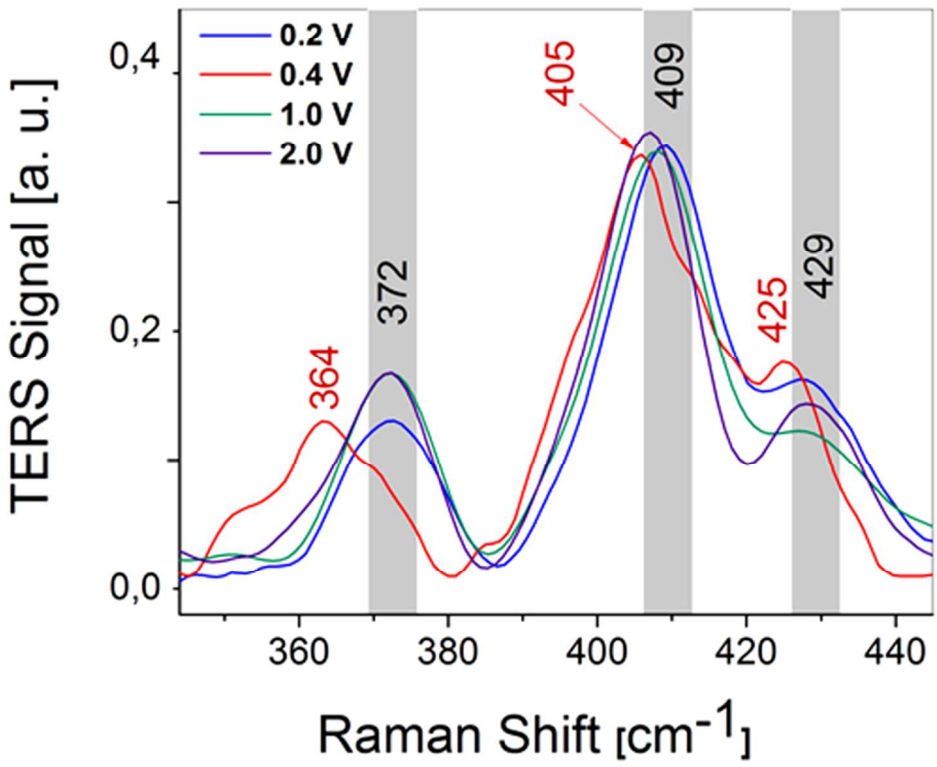

Fig. 6

80x68mm (300 x 300 DPI)

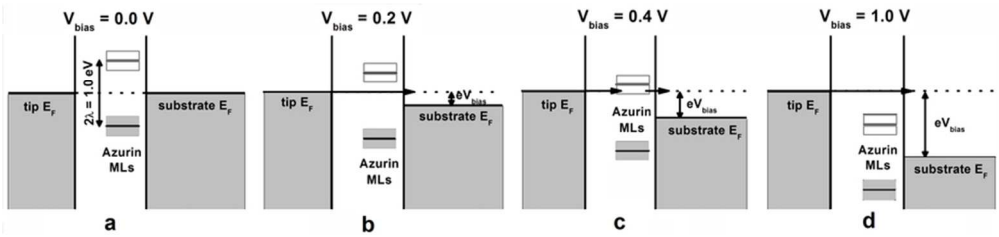

Fig. 7

39x9mm (600 x 600 DPI)

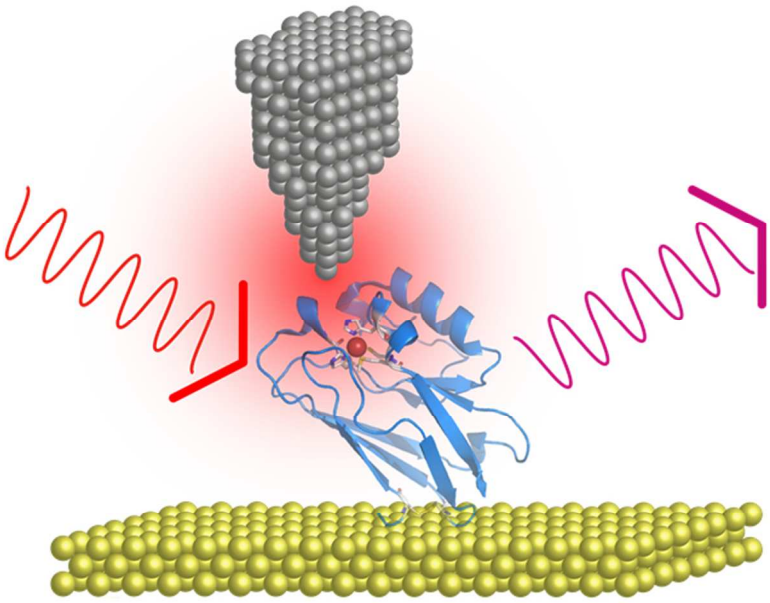

TOC figure

70x54mm (300 x 300 DPI)